J Nanopart Res (2011) 13:6455–6465
DOI 10.1007/s11051-011-0539-0

RESEARCH PAPER

Synthesis, characterisation and functionalisation of luminescent silica nanoparticles

Jessica Labéguerie-Egéa · Helen M. McEvoy · Colette McDonagh

Received: 9 April 2011 / Accepted: 4 August 2011 / Published online: 6 September 2011

Abstract The synthesis of highly monodispersed, homogeneous and stable luminescent silica nanoparticles, synthesized using a process based on the Stöber method is reported here. These particles have been functionalised with the ruthenium and europium complexes: bis (2,2′-bipyridine)-(5-aminophenanthroline) Ru bis (hexafluorophosphate), abbreviated to $(Ru(bpy)_2(phen\text{-}5\text{-}NH_2)(PF_6))$, and tris (dibenzoylmethane)-mono (5-aminophenanthroline) europium(III), abbreviated to (Eu:TDMAP). Both dyes have a free amino group available, facilitating the covalent conjugation of the dyes inside the silica matrix. Due to the covalent bond between the dyes and the silica, no dye leaching or nanoparticle diameter modification was observed. The generic and versatile nature of the synthesis process was demonstrated via the synthesis of both europium and ruthenium-functionalised nanoparticles. Following this, the main emphasis of the study was the characterisation of the luminescence of the ruthenium-functionalised silica nanoparticles, in particular, as a function of surface carboxyl or amino group functionalisation. It was demonstrated that the luminescence of the ruthenium dye is highly affected by the ionic environment at the surface of the nanoparticle, and that these effects can be counteracted by encapsulating the ruthenium-functionalised nanoparticles in a plain 15 nm silica layer. Moreover, the ruthenium-functionalised silica nanoparticles showed high relative brightness compared to the free dye in solution and efficient functionalisation with amino or carboxyl groups. Due to their ease of fabrication and attractive characteristics, the ruthenium-functionalised silica nanoparticles described here have the potential to be highly desirable fluorescent labels, particularly, for biological applications.

Keywords Silica · Nanoparticles · Luminescence · Functionalisation · Biomedical diagnostic · Fluorescent labels · Nanomedicine

J. Labéguerie-Egéa (✉) · H. M. McEvoy · C. McDonagh
Optical Sensors Laboratory, National Centre for Sensor Research, Dublin City University, Glasnevin, Dublin 9, Ireland
e-mail: jessica.egea@dcu.ie

Introduction

Nanoparticles (NPs), for example latex, silica, gold and hybrid particles, have been widely used in biomedical applications. In particular, silica NPs have been used as nanosensors for intracellular sensing and as vectors for drug delivery due to their small size and biocompatibility (Hun et al. 2007; Rosenholm et al. 2010). Silica NPs are also easily functionalised and are stable under most chemical conditions. When functionalised with organic or inorganic luminescent dyes, these NPs have been used as highly bright labels in bioassays (Hashino et al. 2006; Rossi et al. 2006; Jia et al. 2009), as precursors for the preparation of transparent ceramics

for laser or optical applications (Chaim et al. 2010) and as UV absorbers in sunscreen creams (Jaroenworaluck et al. 2006).

The study reported here focused on the synthesis and characterisation of dye-functionalised silica NPs. These NPs are typically synthesized via two main methods; the Stöber method or the microemulsion method (Gao et al. 2009; Kumar et al. 2008; Nooney et al. 2008). The Stöber method is the most suitable method when high yields are required or for applications where NP porosity is important, for example, when the NPs are employed as sensors (Estella et al. 2010). It is also the preferred method for the production of low-cost and environmentally friendly materials, requiring the use of less solvents than the microemulsion method. A modified version of the Stöber method was employed in this study.

The silica NPs in this study were functionalised with the dyes ruthenium bis (2,2′-bipyridine)-(5-aminophenanthroline) Ru bis (hexafluorophosphate), abbreviated to ($Ru(bpy)_2(phen\text{-}5\text{-}NH_2)(PF_6)$), and tris (dibenzoylmethane)-mono (5-aminophenanthroline) europium(III), abbreviated to (Eu:TDMAP). These complexes were chosen due to their high brightness, large Stokes Shift and the possibility to covalently entrap the dyes into the NPs due to their available amino groups. This synthesis is designed to allow covalent entrapment of the dye in the sol–gel matrix which is facilitated by the presence of a COOH group on the dye which reacts with an amino group on the silica precursor. This strategy avoids the leaching of the dye from the NPs and so the luminescence of the particles will remain constant over time (Lei et al. 2006). As far as the authors are aware, fabrication of NPs with covalently entrapped dyes has rarely being carried out using the Stöber method (Nakamura et al. 2007). In his article, Nakamura describes the synthesis of silica NPs using the Stöber method and covalently attached dyes. The main emphasis of his study is the study of fully organic dyes that possess an available ester group that reacts with an available amino group on the silica precursor. In this study, we present the covalent binding of an inorganic dye to a silica network and the reaction between the amino group of the dye and the carboxyl group of the silica precursor.

A large body of work currently exists regarding the functionalisation of NPs, particularly, for use in immunoassays or biological imaging (Wu et al. 2008; Knopp et al. 2009; Louis et al. 2005). In order to be employed in these assays, the NPs need to be functionalised to be covalently conjugated to biological molecules (e.g. antibodies, DNA, proteins etc.). Due to the presence of amino and carboxyl groups on the molecules, functionalisation of NPs with complementary amino or carboxyl groups has been the most popular strategy, as this allows the biological molecules to be directly attached to the NPs using specific linkers such as glutaraldehyde, aminosilanes or via the use of EDC/NHS (An et al. 2007; Hermanson 2008). In this study, the functionalisation of the synthesized NPs using these two popular methods was investigated.

In the first part of this study, we designed a method to obtain luminescent, homogeneous and spherical silica NPs using the Stöber method in which are encapsulated a covalently conjugated dye. We demonstrate that the synthesis technique is generic and can be adapted for encapsulation of two different dyes. In the second part of the study, due to the convenient excitation and emission wavelengths of the ruthenium complex, these NPs were investigated further. The sensitivity of the luminescence intensity to the ionic strength of amino and carboxyl surface functional groups is demonstrated and it is shown that the addition of a plain silica buffer layer serves to eliminate the sensitivity to the surface environment.

Synthesis

The NPs investigated during this study were synthesized using a variation of the Stöber method, which is based on the hydrolysis of a silane in ethanol with ammonia as a catalyst (Stöber et al. 1967).

Dye modification for covalent encapsulation

All chemicals were used as received and purchased from Sigma-Aldrich (Ireland) and Fluorochem (United Kingdom).

The first step of this synthesis was to conjugate the dye ($Ru(bpy)_2(phen\text{-}5\text{-}NH_2)(PF_6)$ or Eu:TDMAP) with carboxyethylsilanetriol. The COOH group of the silane reacted with the NH_2 group of the dye. The silane group remained free for further reaction and creation of the silica network of the NPs. The process is illustrated in the top section of Fig. 1.

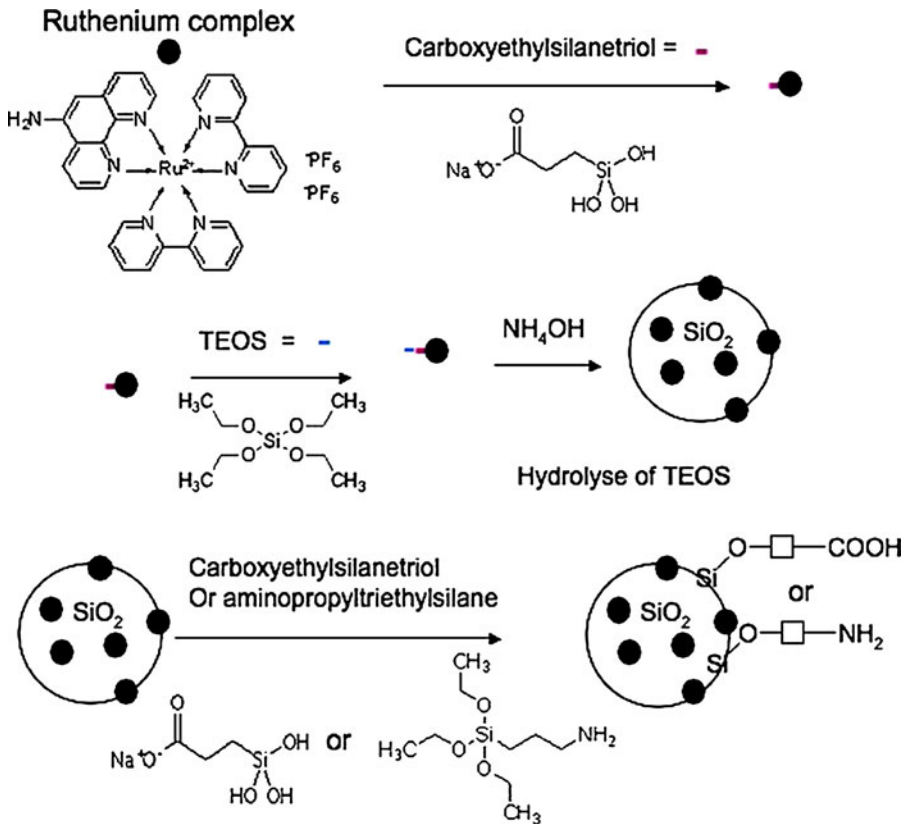

Fig. 1 Modification of the ruthenium dye (*top*), overall synthesis process (*middle*) and surface functionalisation process (*bottom*)

As $Ru(bpy)_2(phen\text{-}5\text{-}NH_2)(PF_6)$ is soluble in water, it was dissolved in 4 mL of water. Eu:TDMAP is soluble in acetone and was therefore first dissolved in 0.5 mL of acetone and then dispersed in 3.5 mL of water. In each case 1.1 mg of the respective dyes were used (1.22 and 1.08 μmol, respectively). Carboxyethylsilanetriol was then added to the dye solution so that the dye covalent conjugation could be performed. This silane has an elevated pH in water (close to 12) and it is known that silanes can hydrolyse in basic conditions. Therefore, the concentration of the silane was kept to 4.10 μL (27.6 μmol) dissolved in 2 mL H_2O. This concentration of silane is low enough to ensure that hydrolysis in water was not induced. The amount of water in the synthesis was controlled so that the silanes were sufficiently condensed to form NPs and not polycations.

The reaction was left under stirring for 24 h, after which, the dye was centrifuged and/or dried and the supernatant discarded. The final step involved the addition of absolute ethanol (5 mL) to dissolve the modified dye. Using this technique, it was possible to obtain ethanol soluble dyes to enable the synthesis via the Stöber method without inducing a modification of the NP formation. Indeed, the proportion of water in the synthesis is a key point in determining the NP diameter. Adding the dye as an ethanol solution does not modify the amount of water in the ammonia solution and, hence, does not affect the NP size.

NP synthesis

NPs with a range of dye concentrations were synthesized in this study. For all syntheses performed, the volume of TEOS was fixed at 0.5 mL (2.24 mmol). The volume of the conjugated dye/ethanol solution was then adapted to produce TEOS/dye molar ratios of 5,000, 10,000 and 20,000 for the ruthenium dye-functionalised NPs and 7,000, europium dye-functionalised NPs. The TEOS/dye mixture in ethanol was stirred for 24 h, after which, due to its high stability, it could be stored for several days before silica NP synthesis. The various steps involved

from dye modification through to silane hydrolysis and finally to formation of the silica NPs are illustrated in Fig. 1.

The TEOS–dye solution was mixed with a certain amount of ammonia (NH_4OH) to hydrolyse the TEOS and obtain silica NPs. The amount of ammonia added was determined by the size of NP desired. During this study, NPs of three different diameters were synthesized, namely, 80, 100 and 120 nm. For each of these particular cases, the quantity of ammonia added was 313, 348 and 411 μL (8.04, 8.94 and 10.55 mmol, respectively). The solution was then left under vigorous stirring for 6 days before washing three times with ethanol and twice with deionised water. The resultant NPs were then stored in deionised water before surface modification.

Addition of a plain outer silica layer to the Ru-NPs

An outer shell of pure silica was added to the ruthenium-functionalised NPs before surface modification with amino or carboxyl groups to investigate the sensitivity of the luminescence to the functional group which is discussed in "Effect of surface modification on the NP luminescence". For the ruthenium-functionalised NPs, a shell of plain silica was added using a protocol adapted from that described by Larson et al. (2008). 10 mg of the dye-functionalised NPs were dispersed in 1 mL of ethanol. Ammonia was then added to the solution using the same quantities as employed in the initial NP synthesis, i.e. 32, 35 and 41 μL (0.82, 0.89 and 1.05 mmol, respectively) of ammonia for 10 mg of NPs of 80, 100 and 120 nm diameters, respectively. Then three aliquots of 17 μL (76.13 μmol) of TEOS were slowly added every 15 min, so that in total 51 μL (228.39 μmol) of TEOS was added. Following this, the solution was stirred for 24 h and washed three times with ethanol. The surface of these particles with outer shell, as well as the particles with no shell, are then functionalised with COOH or NH_2 groups following the protocols described below.

Surface modification

During this study, the synthesized NPs were functionalised with amino groups (NH_2) or carboxyl groups (COOH), as described in the bottom part of Fig. 1.

Functionalisation with carboxyl groups

The carboxyl surface modification process employed was a one-step process. 10 mg of NPs were dispersed in 1 mL of deionised water, to which 40 or 80 μL (269.3 or 538.6 μmol) carboxyethylsilanetriol (salt, 25% in water) was added. Two different volumes of carboxyethylsilanetriol were tested to investigate the effect of surface density of COOH groups. The reaction was left under stirring for 24 h, after which the functionalised NPs were washed three times with deionised water. The NPs were then stored in deionised H_2O for further characterisations.

Functionalisation with amino groups

As with the carboxyl modification, the functionalisation of the NPs with amino groups was also carried out using a one-step process. 5.57 μL (23.8 μmol) of APTES (aminopropyltriethoxysilane) was added to 20 mg of silica NPs dispersed in 1 mL of ethanol. The solution was left stirring overnight, after which, the NPs were washed with ethanol then water and stored in water (An et al. 2007).

Characterisation of the NPs

The synthesized NPs were characterised in terms of size, dispersion, homogeneity and stability using transmission electronic microscopy (TEM), dynamic light scattering (DLS) and zeta potential measurements. A TECNAI 120 (TECNAI) was used for the TEM measurements, and a NanoZS (MALVERN) was employed for the DLS and zeta potential measurements. The NPs were also characterised in terms of luminescence using a spectrophotometer FluoroMax2 (JOBIN–YVON). A fluorescence scanner Infinite M200 (TECAN) was employed to compare the luminescence efficiency of the dye inside the NPs to that of the dye in solution (i.e. relative brightness).

TEM and DLS results

As representative images, the TEM images of both the unfunctionalised and COOH-functionalised Ru-functionalised (TEOS/Ru molar ratio 5,000, diameter 100 nm) are shown in Fig. 2, along with the

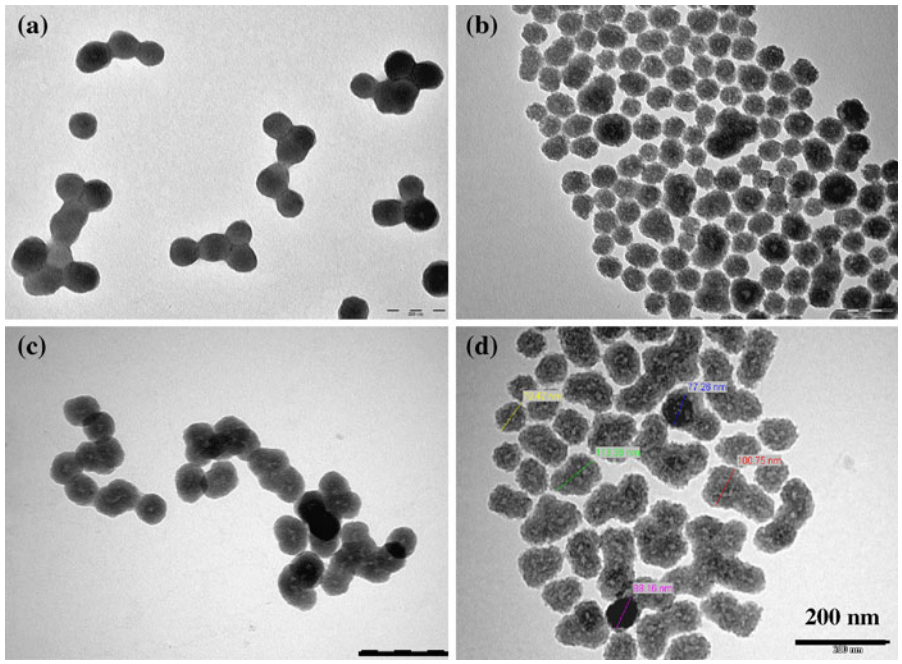

Fig. 2 Ru–SiO_2 and Eu–SiO_2 NPs before (**a** and **c**, respectively) and after (**b** and **d**, respectively) functionalisation with COOH groups. *Scale* 200 nm

unfunctionalised and COOH- and Eu-functionalised NPs (TEOS/Eu molar ratio 7,000, diameter 100 nm).

For both dyes and all molar ratios and NP diameters, it was found that both the unfunctionalised and COOH-functionalised NPs proved to be homogeneous in size and shape, with higher surface roughness evident with the COOH-functionalised NPs. Furthermore, it was found that the size and shape of the NPs were independent of the TEOS/dye molar ratio, i.e. altering the molar ratio did not alter the size of the NPs (which was determined by the quantity of ammonia added during synthesis). It was also found that the NPs were less aggregated following functionalisation. This is also shown by the zeta potential values displayed in Table 1. Indeed, the higher the zeta potential value, the more stable the particles are. Table 1 shows that the COOH-functionalised NPs have a more negative zeta potential than the unfunctionalised NPs. This is due to an increase in the overall charge of the particles in water due to the addition of the negatively charged COOH layer (Knopp et al. 2009).

The results of the DLS and zeta potential (ζ) measurements were in agreement with those of the TEM. Table 1 below contains the results for the unfunctionalised and COOH-surface modified Ru-functionalised NPs (TEOS/Ru molar ratio of 10,000), whilst Table 2 contains the results for the unfunctionalised and COOH-surface modified Eu-functionalised NPs. In both cases, the reported size is the average diameter (the diameters obtain from DLS are calculated based on the number of NPs), for pH 7 diluted NPs solutions in deionised water.

Table 1 Diameters, polydispersity index and zeta potential of Ru–SiO_2 and Ru–SiO_2–COOH NPs as a function of size, for the molar ratio TEOS/Ru = 10,000

RuNPs-expected size	d_{DLS} (nm)	PDI	ζ (mV)
RuNPs-80	90 ± 5	0.1 ± 0.04	−36 ± 6
RuNPs-100	110 ± 20	0.1 ± 0.02	−36 ± 7
RuNPs-120	145 ± 10	0.011 ± 0.001	−50 ± 7
RuNPs-COOH-80	85 ± 10	0.08 ± 0.04	−45 ± 9
RuNPs-COOH-100	100 ± 10	0.032 ± 0.005	−47 ± 8
RuNPs-COOH-120	134 ± 10	0.025 ± 0.002	−51 ± 8

The first column in Table 1 refers to the NP and the expected diameter (based on the synthesis/TEM measurement). As expected, the DLS diameter measurements (column 2) are slightly higher than the

Table 2 Diameters, polydispersity index and zeta potential of Eu:TDMAP–SiO_2 and Eu:TDMAP–SiO_2–COOH NPs as a function of size

EuNPs-expected size	d_{DLS} (nm)	PDI	ζ (mV)
EuNPs-100	105 ± 10	0.05	−45 ± 5
EuNPs-COOH-50	50 ± 5	0.16	−42 ± 4
EuNPs-COOH-100	105 ± 10	0.06	−47 ± 7
EuNPs-COOH-120	130 ± 10	0.2	−49 ± 6

TEM values. This is due to the hydration model that uses the surface hydration to explain this discrepancy of diameters. Indeed, when the NPs are in a liquid, a small quantity of solvent around the particles is displaced when the particle is moving and the DLS measures the displacement of the particle plus the surrounding solvent (Xu 1998; Song and Peng 2005). The DLS gives a value of the hydrodynamic diameter, which is different from the actual diameter which is measured by TEM.

To take into account the corrections needed to get the actual diameter of the NPs from DLS measurements, Eq. 1 (Thomas 1987; Baldi et al. 2007) can be used.

$$d = \frac{d_{DLS}}{(1 + PDI)^5}. \quad (1)$$

This equation allows a good comparison of the diameter obtained from DLS and TEM. For example, using this equation for the Ru-COOH 120 nm NPs (d_{DLS} = 134 nm, PDI = 0.025), the NPs diameter is then 118 nm, which is in good agreement with the TEM measurement (115 nm).

The PDI value (Column 3) represents the homogeneity in size of the NPs. The lower this value, the more monodisperse are the NPs. As observed with the TEM images, the PDI values indicate that there is a high degree of homogeneity for all NP types.

The TEM pictures show slightly aggregated unfunctionalised NPs, compared to little or no aggregation of the COOH-functionalised NPs. This is confirmed by the zeta potential values, which are an indication of the stability of the NPs in water. The more negative or positive the zeta potential, the more the sample is stable and unlikely to aggregate. Zeta potential values around −40/−50 mV, as shown here, indicate stable samples, with slightly lower stability before functionalisation. This is in agreement with the results of the TEM measurements.

The data above demonstrate that the NP synthesis and dye encapsulation method used produces reproducible size, good monodispersity and stability for both dyes and for different dye loadings. The method is generic in nature and can easily be applied to a wide range of dyes to produce NPs with these characteristics.

Luminescence characterisation—Ruthenium-functionalised NPs

In addition to the physical characterisation study, characterisation of the luminescence of samples was also carried out for the NPs that were functionalised with the ruthenium complex. The first phase of this investigation focused on the influence of the NP size on the luminescence signal.

All the samples were characterised using a FluoroMax2 spectrophotometer, with NP concentrations equal to 8×10^{11} NPs/mL and 5 scans per measurement. The concentration has been calculated by measuring the mass of a known volume of NP solution. As the diameter of the NPs is known from DLS and TEM measurements, it is then possible to know the NPs concentration, as detailed below with the Eqs. 2 and 3

$$m_{1NP} = d_{SiO_2} \times V_{1NP} \qquad V_{1NP} = \frac{4}{3}\pi r^3 \quad (2)$$

$$\frac{m_{total,xmL}}{m_{1NP}} = nb_{NPs} \qquad \frac{nb_{NPs}}{V} = C_{NPs}. \quad (3)$$

The excitation wavelength of the dye is 458 nm, and the emission wavelength is 610 nm in pH 7 solution and 600 nm in the silica NP, at pH acid or basic. The data are presented in Fig. 3 below.

As expected, it was observed that the luminescence signal of the dye-functionalised NPs increased as the NP diameter increased. We could observe for this particular dye that the dye loading is not high enough to observe significant luminescence quenching. It is expected that the mean dye–dye separation in the NPs is outside the quenching distance. Based on concentration measurements, there are 640, 1260 and 2200 dye molecules per NP for the 80, 100 and 120 nm NP, respectively.

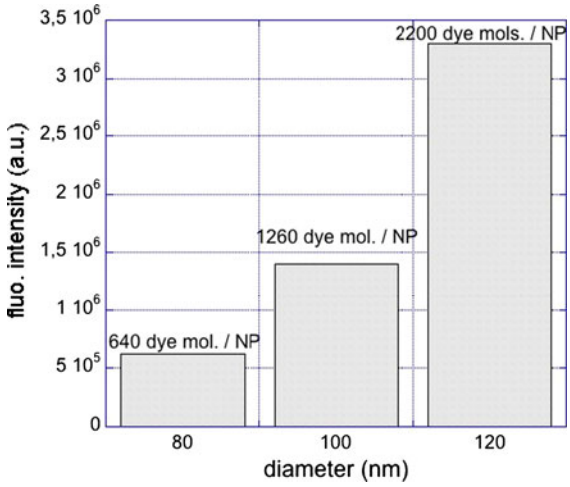

Fig. 3 Luminescence signal for SiO_2–Ru NPs as a function of the NP diameter for a dye loading (TEOS/Ru molar ratio) of 10,000

Following these initial studies, relative brightness measurements were carried out. Using the comparative method described by Fery-Forgues and Lavabre (1999), and employing a scanner, relative brightness measurements were performed on the Ru-functionalised NPs. This method allowed the calculation of the relative brightness of the dye inside the NPs normalized to a single free dye molecule in the solvent. Martini et al. (2009) described that the scattering of silica NPs distorts the brightness measurement by over-estimating it and this was corrected for in this study. To account for this effect, the measurements taken during this study included free dye solution containing plain (no dye functionalisation) silica NPs to compensate for the scattering effect.

A series of diluted solutions of Ru-functionalised silica NPs were prepared, and 250 µL of each dilution was added to the wells of a 96-well Nunc® flat-bottom black plate. The same process was then carried out for the free dye in water solutions, which contained the same concentration of unfunctionalised silica NPs as the dye-functionalised NPs (with matching diameters and PDI values). The NP and dye solutions were diluted until the absorbance of each was below 0.05, to allow a linear behaviour of luminescence versus concentration to be obtained. The luminescence of the solutions was recorded using the Tecan fluorescence scanner.

In order to obtain the values for calculation of the relative brightness, the luminescence of each sample was plotted as a function of the concentration of NPs or dye molecules. Equations 4 and 5 below were then used to calculate the relative brightness:

$$\frac{\mathrm{Fluo_{NP}}}{\mathrm{Fluo_{DYE}}} = \frac{\Phi_{\mathrm{NP}}}{\Phi_{\mathrm{DYE}}} \frac{\mathrm{Abs_{NP}}}{\mathrm{Abs_{DYE}}} \left(\frac{n_{\mathrm{DYE}}}{n_{\mathrm{NP}}}\right)^2 \quad (4)$$

where n is the refractive index of the medium in which the NPs or the dye are dispersed, Φ is the theoretical quantum yield (not referenced for the ruthenium dye studied) and Abs is the absorbance of the NPs or dye molecules.

As both samples in this study were dispersed in water, the ratio between their refractive index is 1, which reduces Formula (4) to the following:

$$\frac{\Phi_{\mathrm{NP}}}{\Phi_{\mathrm{DYE}}} = \frac{\mathrm{Slope_{NP}}}{\mathrm{Slope_{DYE}}}. \quad (5)$$

Hence, the gradient of the intensity versus concentration allows the determination of the relative brightness $\left(\frac{\Phi_{\mathrm{NP}}}{\Phi_{\mathrm{DYE}}}\right)$ using Eq. 5.

As the quantum efficiency of the free dye and dye in NPs is not known, only the relative brightness of the dye inside NPs compared to a single dye molecule in solution can be calculated.

The relative brightness values obtained are presented in Table 3 for Ru-functionalised NPs with diameters of 80, 100 and 120 nm and TEOS/Ru molar ratios of 5,000, 10,000 and 20,000, respectively.

As shown in Table 3, it was found that the NPs presented here have very high brightness values. As expected, the relative brightness was shown to increase as the TEOS/Ru molar ratio decreased, i.e.

Table 3 Relative brightness of the ruthenium-functionalised NPs compared to free dye, as a function of the NP size and dye loading

Sample	Relative brightness
Ru–SiO_2 80 nm–TEOS/Ru 5,000	**2,840**
Ru–SiO_2 100 nm–TEOS/Ru 5,000	**3,891**
Ru–SiO_2 120 nm–TEOS/Ru 5,000	**6,465**
Ru–SiO_2 80 nm–TEOS/Ru 10,000	1,622
Ru–SiO_2 100 nm–TEOS/Ru 10,000	2,138
Ru–SiO_2 120 nm–TEOS/Ru 10,000	3,500
Ru–SiO_2 80 nm–TEOS/Ru 20,000	777
Ru–SiO_2 100 nm–TEOS/Ru 20,000	981
Ru–SiO_2 120 nm–TEOS/Ru 20,000	2251

increased with higher dye concentrations. In agreement with the luminescence results presented above, a linear evolution of the relative brightness was observed for each dye loading as a function of the NPs diameter. Moreover, for the highest dye loading (values in bold characters in Table 3), the relative brightness is particularly high (Sokolov and Volkov 2010). This makes these Ru-functionalised NPs potentially very attractive for a host of applications, particularly, in the important area of biolabeling.

Effect of surface modification on the NP luminescence

Following the luminescence characterisation study, the influence of NP surface modification on luminescence intensity was investigated. The samples were prepared by diluting the NP solution to 8×10^{11} NPs/mL. Each sample was then scanned five times using the FluoroMax2.

In comparison with the unfunctionalised NPs, enhanced luminescence signals were recorded for COOH-modified NPs. The opposite effect was observed for the NPs modified with amino groups, with luminescence signals reduced compared to unfunctionalised NPs. This effect of the luminescence enhancement for COOH-modified NPs and reduction for amino-modified NPs was independent of NP size and TEOS/Ru molar ratio, i.e. both effects recorded for all NP sizes and TEOS/Ru molar ratios. The intensity of TEOS/Ru = 10,000 SiO_2–Ru NPs as a function of NP diameter and surface modification is shown in Fig. 4.

This luminescence enhancement and reduction effects are most likely due to the local charge at the surface of the particles. In water (pH 7), the carboxyl groups are negatively charged (COO^-) as the pK_a of the couple $COOH/COO^-$ is 4.5, whilst for the amino groups, they are positively charged (NH_3^+) as the pK_a is 9.3. This induces a modification of the zeta potential (Table 1) and of the local charge at the surface of the particles, and so the ionic environment of the dye is different. In order to confirm that the effect on the luminescence signal was due to the local charge, the NPs were measured in solutions of pH, which simulated that of the carboxyl and amino groups on the surface, namely, 4.5 for carboxyl and 9.6 for amino groups. pH 7.1 was used to simulate the environment of the unfunctionalised NP.

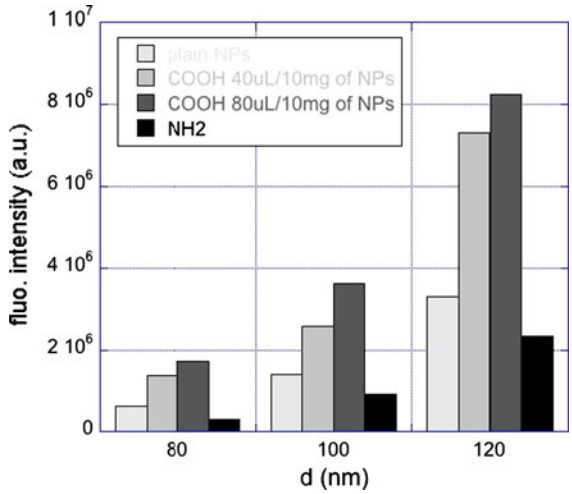

Fig. 4 Luminescence signal of SiO_2–Ru NPs as a function of NP diameter and surface modification for a dye loading of 10,000

Unfunctionalised ruthenium-functionalised silica NPs (80 nm, TEOS/Ru = 5,000) were immersed in the three buffer solutions and the luminescence intensities recorded. Table 4 shows the ratios between the intensity values of the surface-unfunctionalised ("plain") and surface-functionalised ("COOH" or "NH_2") NPs in the relevant pH environment compared to pH of 7.1.

As expected, the same ratio was obtained for plain NPs in pH 7 compared to COOH-functionalised NPs (+ 158%) as was obtained for plain NPs in pH 7 compared to NPs placed in pH 4.5 solution (+158%). This was also the case for the ratio of plain NPs in pH 7 compared to NH_2-functionalised NPs (−34%), which demonstrated a similar ratio to plain NPs in pH 7.1 compared to NPs in pH 9.6 solution (−26%). These results confirm that the pH has a significant influence on the enhancement or quenching of the luminescence of the NPs. Simulating the pH of the equivalent charge of the carboxyl and amino groups in solution results in similar effects on the luminescence signal, thus confirming that the pH changes the ionic charge surrounding the NPs and, hence, the behaviour of the dye.

In order to investigate this behaviour further, the Ru-functionalised SiO_2 NPs were encapsulated in a 15 nm plain silica shell. This resulted in NPs with core–shell structures, as seen in the TEM image in Fig. 5. The darker core, compared to the lighter shell, is due to the stronger contrast of the ruthenium

Table 4 Ratio between the luminescence intensity at 600 of 80 nm Ru–SiO_2 NPs, with NH_2 or COOH groups or unfunctionalised, and in different pH solutions (pH = 4.5, 7.1 and 9.6)

Types of NPs	COOH-functionalised	NH_2-functionalised	pH 4.5	pH 9.6	+15 nm silica shell +COOH-functionalised	+15 nm silica shell +NH_2-functionalised
Increase of the intensity versus plain NPs at pH 7.1 (%)	+158	−34	+158	−26	−17	−19

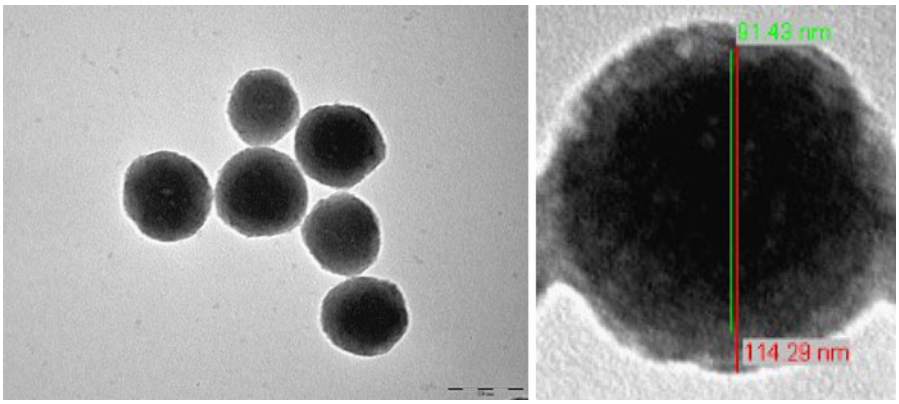

Fig. 5 Ruthenium-functionalised silica NPs, coated with shells of plain silica

complex encapsulated in the NPs presenting a higher electron density than plain silica. Shells of 15 nm thickness were observed for all imaged NPs.

The core–shell NPs were functionalised with carboxyl and amino groups as described above. Luminescence measurements were then performed with 0.5 mg/mL solutions and scanned using the FluoroMax2. The intensities of the functionalised NPs were compared with those of the unfunctionalised and functionalised core–shell NPs.

It was found that the addition of the shell significantly reduced the variation in luminescence intensity recorded for the surface-functionalised NPs versus the unfunctionalised NPs. For the dye-functionalised silica NPs without a shell, the increase or decrease in luminescence signal between the plain NPs (Fig. 4, first bar) and the COOH-functionalised NPs (Fig. 4, third bar) and NH_2-functionalised NPs (Fig. 4, fourth bar) is calculated to be +158% and −34%. However, this variation was significantly reduced for the NPs encapsulated in a silica shell, with values of −17% following carboxyl functionalisation and −19% following amino functionalisation (columns 6 and 7 of Table 4). Screening the ruthenium dye by a pure silica shell reduced the influence of the functionalisation on the dye. Therefore, it was concluded that the enhancement or quenching of luminescence observed after surface functionalisation was influenced by the type of groups at the surface of the particles and it was primarily the dyes at the surface of the NPs that were influenced rather than the dye molecules inside the particles. Indeed, according to Witschger (2008), for a 100 nm NP with a surface to volume ratio of 60,000,000 m^2/m^3, as our NPs, the fraction of molecules at the surface of the NP is about 55%. For our 100 nm NP, this means that about 700 dye molecules (Fig. 3) are at the surface of the NP against 500 in the volume. A large amount of the dye molecules are then affected by the surface functionalisation. When these particles are encapsulated in a plain silica shell, the dye molecules are no more affected; they all belong to the volume of the particle. Thus, the values obtained for the modification of the luminescence after surface modification is decreased.

Conclusion

A novel protocol involving a modified Stöber method to obtain bright dye-functionalised silica NPs

conjugated with TEOS was presented. The particles produced are highly uniform, spherical, monodispersed and homogeneous in size and stable. The ruthenium-functionalised NPs have high-luminescence intensity and can be easily and efficiently functionalised with carboxyl and amino groups, making them very attractive for a wide range of uses, including biological labeling.

The luminescence of the NPs was shown to be enhanced in the presence of surface carboxyl groups and was quenched when the NP surface was functionalised with amino groups. This effect was explained in terms of the differing charge environment experienced by the dye under the conditions of functionalisation. Furthermore, this conclusion was corroborated by monitoring the NP luminescence in pH environments that simulated the charge due to the functional groups. The effect was successfully eliminated by the addition of a thin protective pure silica shell on the NP. Whilst the detailed mechanism of this quenching/enhancement effect is still under investigation, the study presented here could be successfully exploited in a range of applications including use of high brightness NPs as labels for enhanced luminescence-based bioassays as well as in intracellular diagnostics.

Acknowledgments The authors would like to thank Tiina Toivonen from the Electron Microscopy Laboratory, University College Dublin for the TEM pictures and Dr. Martin Schulz and Professor Han Vos for useful discussions. This study was funded in party by the European Commission under the Seventh Framework Programme within the research project NANOMUBIOP (Enhanced sensitivity Nanotechnology-based Multiplexed Bioassay Platform for diagnostic applications).

References

An Y, Chen M, Xue Q, Liu W (2007) Preparation and self-assembly of carboxylic acid-functionalized silica. J Colloids Interface Sci 311:507–513

Baldi G, Bonacchi D, Franchini MC, Gentili D, Lorenzi G, Ricci A, Ravagli C (2007) Synthesis and coating of cobalt ferrite nanoparticles: a first step toward the obtainment of new magnetic nanocarriers. Langmuir 23:4026–4028

Chaim R, Marder R, Estournès C (2010) Optically transparent ceramics by park plasma sintering of oxide nanoparticles. Scr Mater 63:211–214

Estella J, Wencel D, Moore JP, Sourdaine M, McDonagh C (2010) Fabrication and performance evaluation of highly sensitive hybrid sol-gel derived oxygen sensor films based on fluorinated precursor. Anal Chim Acta 666:83–90

Fery-Forgues S, Lavabre D (1999) Are fluorescence quantum yields so tricky to measure? A demonstration using familiar stationery products. J Chem Educ 76:1260–1264

Gao XQ, He J, Deng L, Cao HN (2009) Synthesis and characterization of functionalized rhodamine B-doped silica nanoparticles. Opt Mater 31:1715–1719

Hashino K, Ito M, Ikawa K, Hosoya C, Nishioka T, Mastumoto K (2006) Application of a lanthanide fluorescent chelate label for detection of single-nucleotide mutations with peptide nucleic acid probes. Anal Biochem 355:278–284

Hermanson GT (2008) Bioconjugate techniques, 2nd edn. Academic Press, San Diego, CA, p 574

Hun X, Zhang Z (2007) Preparation of a novel fluorescence nanosensor based on calcein-doped silica nanoparticles, and its application to the determination of calcium in blood serum. Microchim Acta 159:255–261

Jaroenworaluck A, Sunsaneeyametha W, Kosachan N, Stevens R (2006) Characteristics of silica-coated TiO_2 and its UV absorption for sunscreen cosmetic applications. Surf Interface Anal 38:473–477

Jia TT, Cai ZM, Chen XM, Lin ZJ, Huang XL, Chen X, Chen GN (2009) Electrogenerated chemiluminescence ethanol biosensor based on alcohol dehydrogenase functionalized $Ru(bpy)_3^{2+}$ doped silica nanoparticles. Biosens Bioelectron 25:263–267

Knopp D, Tang D, Niessner R (2009) Review: bioanalytical applications of biomolecule-functionallized nanometer-sized doped silica particles. Anal Chim Acta 647:14–30

Kumar R, Roy I, Ohulchanskyy TY, Goswami LN, Bonoiu AC, Bergey EJ, Tramposch KM, Maitra A, Prasad PN (2008) Covalently dye-linked, surface-controlled, and bioconjugated organically modified silica nanoparticles as targeted probes for optical imaging. ACS Nano 2:449–456

Larson DR, Ow H, Vishwasrao HD, Heikal AA, Wiesner V, Webb WW (2008) Silica nanoparticle architecture determines radiative properties of encapsulated fluorophores. Chem Mater 20:2677–2684

Lei B, Li B, Zhang H, Lu S, Zheng Z, Li W, Wang Y (2006) Mesostructured silica chemically doped with RuII as a superior optical oxygen sensor. Adv Funct Mater 16:1883

Louis C, Bazzi R, Marquette CA, Bridot J-L, Roux S, Ledoux G, Mercier B, Blum L, Perriat P, Tillement O (2005) Nanosized hybrid particles with double luminescence for biological labelling. Chem Mater 17:1673–1682

Martini M, Montagna M, Ou M (2009) How to measure quantum yields in scattering media: application to the quantum yield measurement of fluorescein molecules encapsulated in sub-100 nm silica particles. J Appl Phys 106(9):094304–094313

Nakamura M, Shono M, Ishimura K (2007) Synthesis, characterization, and biological applications of multifluorescent silica nanoparticles. Anal Chem 79:6507–6514

Nooney RI, McCahey CMN, Stranik O, Le Guevel X, McDonagh C, MacCraith BD (2008) Experimental and theoretical studies of the optimization of fluorescence from near-infrared dye-doped silica nanoparticles. Anal Bioanal Chem 393:1143–1149

Rosenholm JM, Sahlgreen C, Lindén M (2010) Towards multifunctional, targeted drug delivery systems using mesoporous silica nanoparticles—opportunities & challenges. Nanoscale 2:1870–1883

Rossi LM, Shi LF, Rosenzweig N, Rosenzweig Z (2006) Fluorescent silica nanospheres for digital counting bioassay of the breast cancer marker HER2/nue. Biosens Bioelectron 21:1900–1906

Sokolov I, Volkov DO (2010) Ultrabright fluorescent mesoporous silica particles. J Mater Chem 20:4247–4250

Song S, Peng C (2005) Thickness of solvation layers on nanoscale silica in water and ethanol. J Dispers Sci Technol 26:197–201

Stöber W, Fink A, Bohn E (1967) Controlled growth of monodisperse silica spheres in the micron size range. J Colloid Interface Sci 26:62–69

Thomas JC (1987) The determination of Log normal particle size distributions by dynamic light scattering. J Colloid Interface Sci 117:187–192

Witschger O (2008) www.sante-travail-lyon.org/diaporamas/mdt-lyon-exposition-ow.pdf

Wu H, Huo Q, Varnum S, Wang J, Liu G, Nie Z, Liu J, Lin Y (2008) Dye-doped silica nanoparticle labels/protein microarray for detection of protein biomarkers. Analyst 133:1550–1555

Xu R (1998) Shear plane and hydrodynamic diameter of microspheres in suspension. Langmuir 14:2593–2597